SoRo

Soft Robotics

Open camera or QR reader and
scan code to access this article
and other resources online.

A Method for 3D Printing and Rapid Prototyping of Fieldable Untethered Soft Robots

Zach J. Patterson,[1,*] Dinesh K. Patel,[2,*] Sarah Bergbreiter,[1,3] Lining Yao,[1,2] and Carmel Majidi[1,3]

Abstract

Because they are made of elastically deformable and compliant materials, soft robots can passively change shape and conform to their environment, providing potential advantages over traditional robotics approaches. However, existing manufacturing workflows are often labor intensive and limited in their ability to create highly integrated three-dimensional (3D) heterogeneous material systems. In this study, we address this with a streamlined workflow to produce field-deployable soft robots based on 3D printing with digital light processing (DLP) of silicone-like soft materials. DLP-based 3D printing is used to create soft actuators (2.2 g) capable of exerting up to 0.5 Newtons of force that are integrated into a bioinspired untethered soft robot. The robot walks underwater at speeds comparable with its biological analog, the brittle star. Using a model-free planning algorithm and feedback, the robot follows remote commands to move to desired positions. Moreover, we show that the robot is able to perform untethered locomotion outside of a laboratory and in a natural aquatic environment. Our results represent progress in soft robot manufacturing autonomy for a 3D printed untethered soft robot.

Keywords: 3D printed soft robots, untethered, bioinspired

Introduction

INSPIRED BY SOFT ORGANISMS in nature, soft robots have seen a resurgence in recent years thanks to the potential for more lifelike, more adaptable, and safer systems.[1–3] They have also shown promise in exploration of underwater environments.[4] Rather than using rigid linkages connected by motorized joints, as in traditional robots, soft robots incorporate more flexible and compliant materials, such as silicone rubber.[5] Usually, these robots are fabricated in complex custom molds.[6,7] Although replica molding has the potential to scale well for industrial scale manufacturing and are compatible with popular materials such as silicone, they have several distinct disadvantages.

First, design versatility is limited to moldable geometries: stark overhangs, thin walls, and complex internal geometries present significant problem.[8] Practically, the mold design task presents significant design and engineering overhead. In addition, iteration upon an early-stage design requires producing a new mold for each prototype, a process that can be time consuming and expensive. Together, these issues impair

[1]Department of Mechanical Engineering, Carnegie Mellon University, Pittsburgh, Pennsylvania, USA.
[2]Human-Computer Interaction Institute, Carnegie Mellon University, Pittsburgh, Pennsylvania, USA.
[3]The Robotics Institute, Carnegie Mellon University, Pittsburgh, Pennsylvania, USA.
*These authors contributed equally to this study.

the ability of many practitioners in the field to create soft robots with complex three-dimensional (3D) structures and rapidly iterate through design.

Additive manufacturing (AM) methods such as 3D printing have the potential to alleviate the aforementioned issues through direct write fabrication processes, which can save time and labor and reduce the number of steps for fabrication.[9] However, despite its tremendous promise and potential, 3D printing has not yet been widely adopted in the fabrication of soft robotic systems.[10] Many factors may play a role, but one important reason lies in the limited mechanical properties of the soft materials that are printable with commercial 3D printing systems. To overcome this, researchers have used direct ink write 3D printing technology for printing silicones. However, these need hours to cure and the lateral resolution is determined by the size of printing nozzle.[11]

Another disadvantage of this technique is that it requires a support bath for printing overhang structures, which limits the use of these technique for fabricating structures with high complexity.[12] There are other printing platforms that can be used for printing elastomers or soft materials. These include digital light processing (DLP), stereolithography, polyjet, and binder jetting. Compared with other techniques, DLP-based 3D printing is relatively low cost and high throughput. Printing takes place in a liquid environment comprising monomers, cross-linker, and photoinitiators. It can generate highly complex structures with overhangs at multiple scales with submicrometer resolution. In recent years, researchers have made advancement in DLP-based 3D printing such as continuous liquid interface production enabling 100 times faster printing,[13] projection micro-stereolithography (p-μSLA)

providing micro to submicrometer printing resolution,[14] and large-area p-μSLA creating 3D features spanning from nanometers to centimeters.[15]

In this study, we contribute a pipeline for rapid prototyping of fieldable untethered soft robots with 3D printed elastomer. This study leverages recent methods developed by Patel *et al.* for printing a stretchable and UV-curable (SUV) elastomeric resin with tunable mechanical properties and elongation at break from 240% to 1100%,[16] which is yet to be leveraged to develop fully autonomous soft robots. Referring to Figure 1A and B, we use DLP to print the resin and create elastomeric structures that have silicone-like compliance and elasticity.

Leveraging the high printing resolution (100 μm along Z and 27 μm along X–Y), we design and print a dedicated structure to embody and fix shape memory alloy (SMA) coils. The 3D printed structures with embedded SMA function as soft robot actuators that have low stiffness and are highly deformable (Fig. 1C). With this manufacturing approach, we are able to create untethered soft robots, such as the legged robot shown in Figure 1D–F inspired by the brittle star. Although the design is similar to previously reported robots,[17] the specifics of this design is not the contribution.

This study advances the fields of soft robotics and AM by introducing a workflow that uniquely combines DLP-based 3D printing, soft and elastic rubber, untethered soft robot functionality, and bioinspired mobility. Previous efforts at 3D printed soft robots have largely focused on implementations that are tethered,[11] that is, the robot's power source and/or control electronics are located away from the robot. Although this makes sense in many applied contexts—for example, pipe exploration, hospitals, and nuclear facilities—it is disadvantageous for a mobile and autonomous robot meant to traverse unstructured terrain.[18]
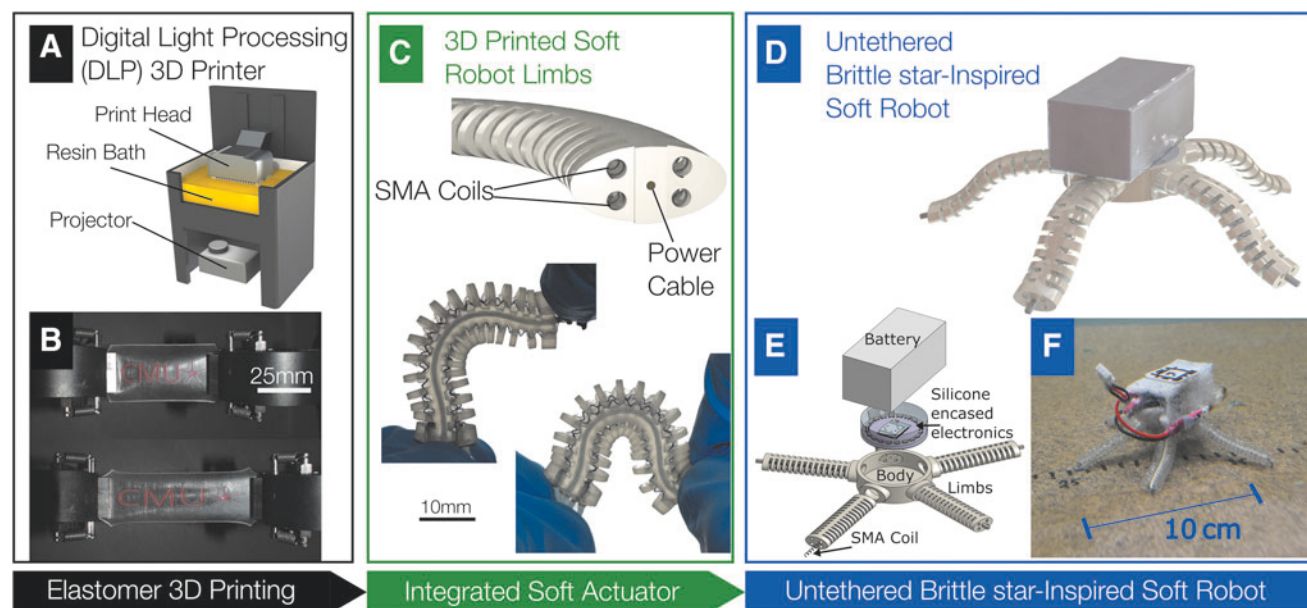

FIG. 1. Fabrication process for 3D printed robot. (**A**) Rendered depiction of the printer with the critical components labeled. (**B**) Rubber-like 3D printed elastomer at 0% and 100% extension. (**C**) *Top*: Rendered model of a cut section of the actuator to highlight the location of several important features, including the SMA, power wire (connecting to the positive terminal of the battery), and notches. *Bottom*: Photos of deformed actuators to showcase flexibility. (**D**) Robot CAD Rendering. (**E**) Explosion of robot features showing the critical components of the robot. (**F**) Photo of the robot sitting in a tank. 3D, three-dimensional; CAD, computed aided design; CMU, Carnegie Mellon University; SMA, shape memory alloy.
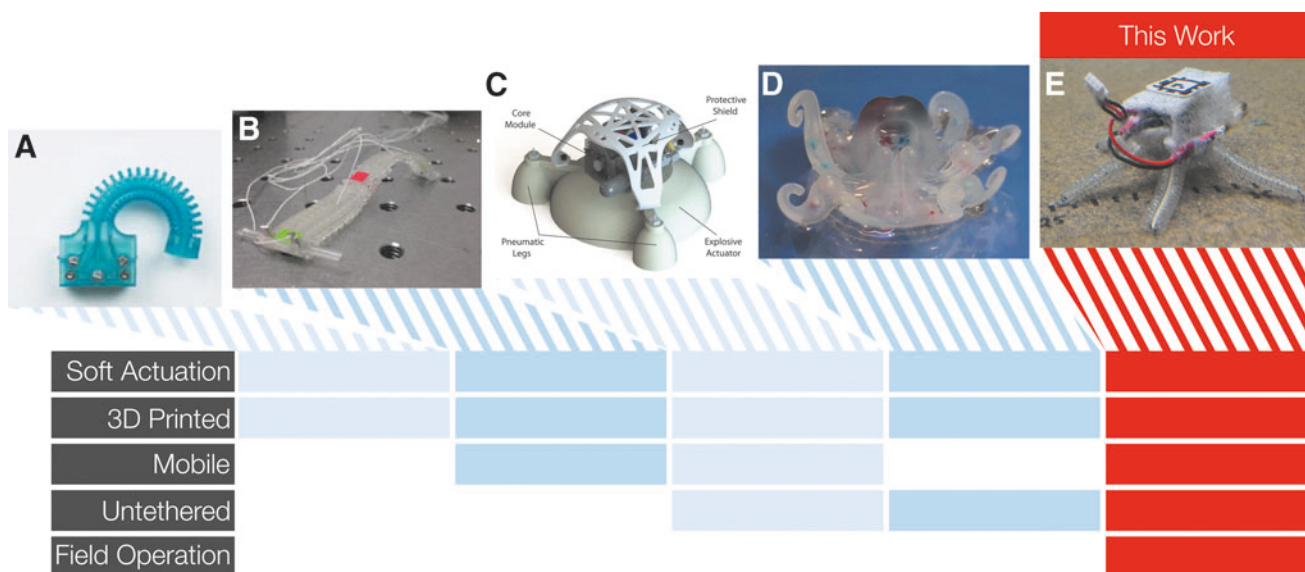
FIG. 2. Progression of soft robotics engineering. **(A)** Single 3D printed soft actuator.[28] **(B)** Tethered 3D printed soft robot.[44] **(C)** Untethered robot with rigid and flexible components.[23] **(D)** Fully untethered and autonomous 3D printed soft robot without mobility.[19] **(E)** This study builds off previous work by combining untethered mobility and feedback to enable autonomous goal-oriented behavior and performance in unstructured environments outside the laboratory.

Although there are examples of 3D printed systems that are untethered,[19–23] these are not mobile robots that are capable of performing controlled goal-oriented locomotion tasks.[24–27] In addition, in this study we demonstrate preliminary results of robot performing in a natural environment. Referring to Figure 2, the manufacturing workflow presented in this article is capable of producing bioinspired robots that captures all aspects of soft actuation, mobility, untethered functionality, field operation, and 3D printed elastic elements.

Materials and Methods

3D printing and robot fabrication

The soft robot is composed of elastomeric limbs that are embedded with coils of nickel–titanium SMA. When electrical current is supplied to the SMA, the coils contract and cause the limb to bend in a prescribed direction. As shown in Figure 1C, each limb actuator contains four SMA coils, which allow for bi-directional motion in and out of the plane. This approach to creating SMA-powered soft robot limbs is based on design principles previously reported in Patterson et al.[17] and Walters and McGoran.[28]

Referring to Figure 1C, the soft robot limbs are 4.5 cm long 3D elastomeric structures with ellipsoid cross sections (12×6 cm) composed of outer notches and inner channels (in which the SMA coils are inserted). The notches reduce the actuator's mechanical resistance to bending by reducing the amount of material that must be deformed for a given actuator bend angle. Figure 1C (top) shows a rendering of the design, highlighting the critical features and Supplementary Figure S1 shows a detailed engineering drawing. The actuators are 3D printed using a DLP-based 3D printer (PicoHD@27, Asiga) using a SUV elastomeric resin.

The elastomeric resin used for 3D printing consists of epoxy aliphatic acrylate (EAA; Ebecryl 113, Allnex USA) and aliphatic urethane di-acrylate (AUD; Ebecryl 8413,

Allnex, USA) in ratio 1:1 by wt. 2% Diphenyl(2,4,6-trimethylbenzoyl)phosphine oxide (TPO; Genocure TPO, RAHN USA Corp.) of total weight of the polymeric/elastomeric resin was added as the photoinitiator. The printer is a top–down DLP system with a digital mirror device and a ultraviolet light emitting diode (UV–LED) light source operating at 385 nm. The printer was maintained at 42°C during printing and each layer was irradiated for 1 s and layer thickness was 100 μm.

The detailed printing parameters are included in Supplementary Data, Supplementary Table S1. The printed structures were sonicated with isopropyl alcohol for 3 min to remove uncured resin followed by a 5 min postcuring in a UV oven (UVP CL-1000 UV Oven). Supplementary Figure S4A shows a stress–strain curve for a dog bone-shaped sample (ASTM D412) of elastomer printed using this technique. It was observed that the strain at failure is ~240% (Supplementary Fig. S4A). This particular material was chosen because of its high similarity to conventional silicone rubber, especially in its hyperelastic material response. The material is closer to silicone rubber than commercial 3D printed rubbers such as thermoplastic urethane (TPU).

After printing the actuator form factor, SMA coils are stretched and cut to size (~40 mm). They are inserted into their respective holes in the printed part. At the distal end of the actuator, they are crimped together with the central wire. At the proximal end, they are each crimped to an individual wire. A dab of fast cure one-part super glue (Loctite Gel) is placed at each crimp to secure it to the actuator.

The manufacturing method introduced here is used to create a soft robot inspired by the brittle star, a mobile species of sea star that uses its flexible arms to pull itself along the ocean floor. In contrast to a previous implementation,[17] which we produced using conventional elastomer molding methods, the 3D printing approach developed here enabled us to implement a much smaller design (that would be difficult

or infeasible with casting techniques) inspired by smaller brittle star species, such as Ophioderma appressum.[29] Despite its small size, the robot is fully untethered—that is, contains all necessary power and control electronics onboard. After all actuators are fully fabricated, five of them are connected to a custom printed circuit board (PCB). The PCB contains the microcontroller (BL652 SoC with nRF52832), transistors for control of the SMA, and voltage regulation to step the 7.4 V battery down to 3.3V for the microcontroller.

The PCB is then sealed in silicone (Smooth-On Dragon-Skin 10) to prevent water damage. The actuators and sealed PCB are then inserted into the 3D printed robot body. An off-the-shelf drone battery (Venom Fly 30C 2S 300mAh) is waterproofed with a liquid rubber sealant (Flex Seal) before being cast in foam (Smooth-On Soma Foama 15) to reduce the effective weight in the water. Finally, An AprilTag fiducial[30] is placed at the top of the robot for visual tracking (Fig. 1F). Overall, the robot is 12.4 cm in diameter, has a mass of 65 g, and has an overall specific gravity of 1.15.

To activate an actuator, the microcontroller sends a signal to the transistor gate, which pulls one end of the SMA to ground, whereas the other is held at 7.4V by the battery. The amount of time that the gate is held high on the resistor, which we call activation time, is proportional to the current that is provided to the SMA. Because the SMA has a given resis-

tance, the current produces Joule heating, which causes the SMA to undergo a phase change from the compliant detwinned martensite phase to the stiff austenite phase. This phase change is accompanied by a macroscopic contraction. Therefore, the activation time is proportional to the force and the strain produced by the actuator.

Robot experimental setup

The robot functions using similar locomotion gaits to the brittle star. These gaits are based on the pentaradial symmetry of the brittle star morphology in which each limb is equally equipped to be the "front" or the "leading limb."[31] After the identity of the leading limb is determined, the two limbs adjacent to that limb are moved in a "rowing" motion, pulling the robot or organism along the substrate. The three remaining limbs remain passive. Figure 3A shows a diagram of a single gait cycle under this locomotion scheme. The arms swing forward and then down to push the robot off the surface before swinging back to push the robot forward. To accomplish this gait, a set of SMA activation times, the control input in this study, is determined by trial and error (Fig. 3B, C).

Using Ohm's law and given the specifications of the battery, the measured resistance of the SMA circuit (3Ω), and the timing characteristics of the gait, power consumption and
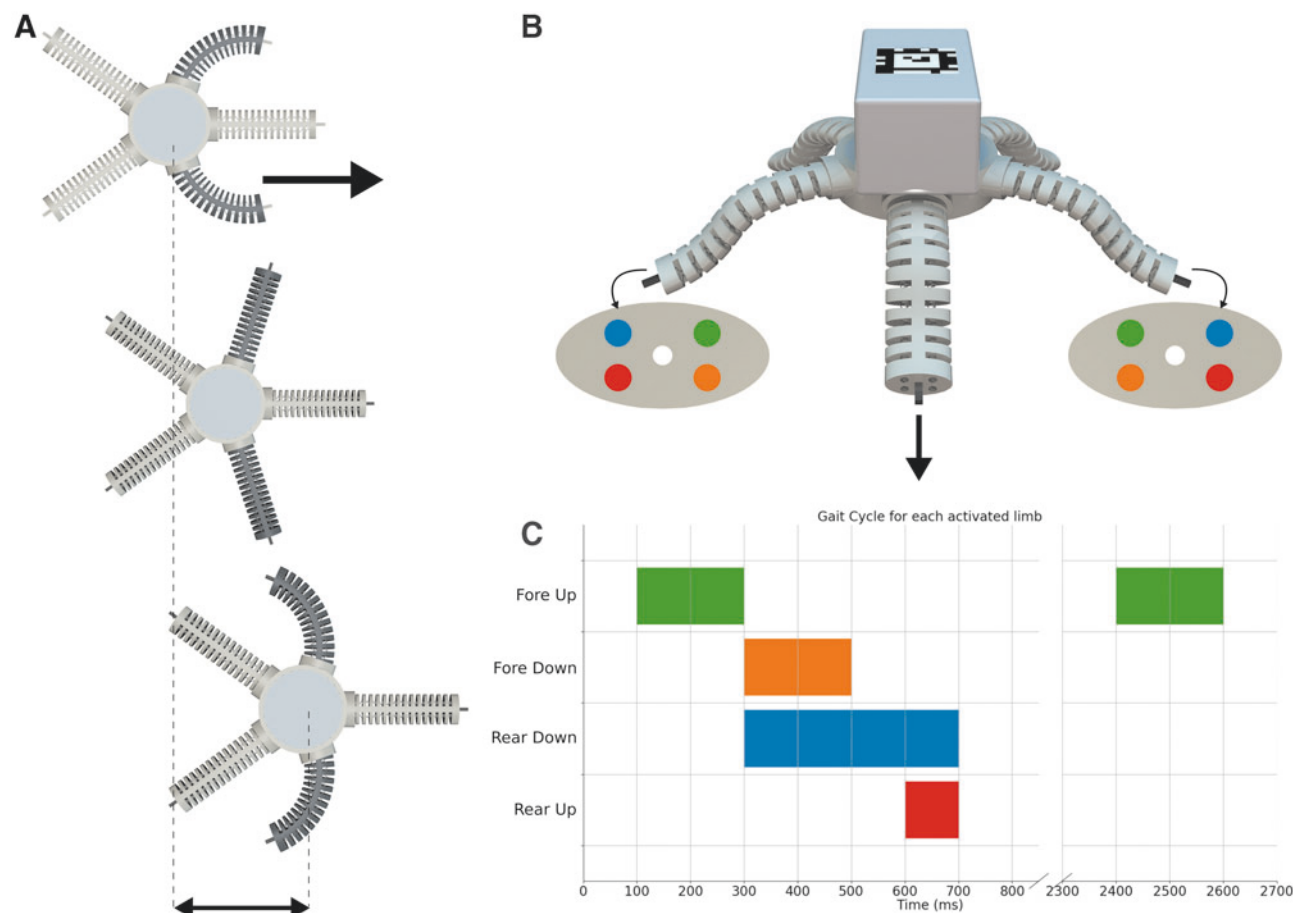

FIG. 3. Robot gait. **(A)** The robot moves forward with a bioinspired rowing gait during which the arms to either side of the "leading limb" are swung forward and planted in the ground before pulling the body forward. **(B)** Sequence of inputs to the SMA actuators for each of the active limbs during a single gait cycle. **(C)** Shows the position of the SMAs for the presented gait cycle.

battery life of the robot can be estimated. Based on this, the power for a single actuation is found to be 18.25W, whereas the average power over a gait cycle is 6.85W. With the used battery, operation time for a single charge at this gait is about 20 min.

The feedback control algorithm is described as follows. A target position is selected by the operator by clicking on a display of the environment. The planner considers five potential actions, or motion primitives, one corresponding to the direction of each limb. The camera finds the position and orientation of the Apriltag fiducial. A transition model is then used to find the action expected to minimize the distance to the target. This transition model essentially states that the motion primitive will move the robot 2 cm in the direction of the limb corresponding to that primitive, without changing direction. This results in a greedy policy where the planner only considers the effect of the action on the next state. The algorithm is formally specified in Algorithm 1.

Algorithm 1: A greedy model-based policy

Input : Robot state $\mathbf{x}_t$, goal position $\bar{\mathbf{x}}$, goal threshold ϵ, set of primitives $\mathbf{a} \in \mathcal{A} = \{\mathbf{a}^0, \mathbf{a}^1, \mathbf{a}^2, \mathbf{a}^3, \mathbf{a}^4\}$, transition function $\mathbf{x}_{t+1} = \mathbf{x}_t + F(\mathbf{x}_t, \mathbf{a}_t)$, tolerance d for distance to goal

Output: Closed loop trajectory of motion primitives $\mathbf{a}_t$ to get to the goal

1 $\bar{\mathbf{x}} \leftarrow$ Operator.input()
2 **while** $||\mathbf{x}_t - \bar{\mathbf{x}} + \epsilon||_2 > d$ **do**
3   **for** $\mathbf{a}^i \in \mathcal{A}$ **do**
4      $\hat{\mathbf{x}}_{t+1} = \mathbf{x}_t + F(\mathbf{x}_t, \mathbf{a}^i)$
5      $c(\hat{\mathbf{x}}_{t+1}) = ||\hat{\mathbf{x}}_{t+1} - \bar{\mathbf{x}}||_2$
6   **end**
7    $\mathbf{a}^t = \underset{\mathbf{a}^i}{\arg\min}\, c(\hat{\mathbf{x}}_{t+1})$
8    $\mathbf{x}_{t+1} \leftarrow$ Robot.execute($\mathbf{a}^t$)
9    $\bar{\mathbf{x}} \leftarrow$ Operator.input()
10 **end**

The robot runs a custom microcontroller program that controls the limbs. It receives instructions for input identity and magnitude through Bluetooth Low Energy (BLE) from a remote microcontroller (also nRF52832). This remote microcontroller receives these instructions through the serial port from custom Python scripts on an Ubuntu computer.

The robot can move in the open loop in any underwater environment. In our test setup, we included an overhead camera (Intel Realsense D435) to enable feedback. The camera is placed ~ 54.3 cm above the container that is used for the water tank. A piece of Rock-on-a-Roll from Aquatica Water Gardens covers the bottom of the tank to provide a more frictional surface than the bare plastic. Performance of the robot on Rock-on-a-Roll versus bare plastic is presented in Supplementary Figure S7. A remote computer running the software stack is nearby and is connected to the remote microcontroller. Of course, Bluetooth transmission is woefully short-range through water. We observe that it rapidly degrades for this robot over a distance of 30 cm in water. Therefore, for extended operation at realistic depths, the gait must be hard coded into

the robot. A second camera is placed in front of the container on a tripod to capture high-resolution footage. See Supplementary Figure S5 for a photo and schematic of this setup.

To conduct the field tests of the robot, the robot was transported to Panther Hollow Lake in Schenley Park in Pittsburgh, USA. The robot was placed in the water and instructed to move using one of its motion primitives. A GoPro Hero 2 Camera attached to a tripod was used to capture the video underwater.

Results

Actuator characterization

To gauge actuator performance, the elastomer material and the actuators were put through a battery of tests. First, a blocking force test was performed on the fabricated actuator to get an understanding of the actuator force output. The blocking force is relevant because the resulting force is the upper bound of force output that can be commanded during locomotion. The actuators are actuated while up against a force plate to prevent motion. The actuator is clamped to an acrylic fixture that is held in place by the Instron clamp (see schematic in Fig. 4A inset and photo in Supplementary Fig. S2). An acrylic plate is affixed to a universal testing machine (Instron 5969, 10 N load cell).

The actuator is then activated for various levels of the input and the data are collected by the Instron DAQ. Matlab was used for postprocessing. In this study, we use activation time as our control input to keep the results consistent with the control input of the robot, which is presented in the following subsections. We vary the activation time from 50 to 300 ms. Results from the blocking force test for 11 actuators are shown in Figure 4A, whereas a schematic of the test setup is displayed as an inset. It was observed that as the activation time is increased, the blocking force also increases with a roughly linear dependency. With activation times of 200 and 300 ms, the observed blocking force is $\sim 0.45 \pm 0.09$ N and 0.5 ± 0.14 N, respectively.

Using the same blocking force test, a longer-duration test was performed on a single actuator to determine any degradation of performance after multiple cycles (Fig. 4B). The actuator was periodically activated with a 70-ms pulse every 10 s for >2500 cycles. These activation parameters were set to ensure that the actuator can fully cool before an additional actuation to prevent thermal buildup. It was observed that beyond 2600 cycles, the device was functional and producing similar forces.

Next the forces of the actuators are characterized in a more realistic scenario where the actuator is activated tangentially to the ground. Ideally, the actuator sticks due to frictional forces. To collect force data, an ATI Nano17 6 axis transducer is attached to a custom 3D printed plastic (VeroWhite) plate and bolted to an optical table. The actuator is held parallel to the plate and is lowered until just touching. We then program a similar gait as described for the robot and record forces from the plate. This test is performed on the high-friction Rock-on-a-Roll surface and on smooth Vero-White, with results plotted in Figure 4C.

The actuator's angular displacement is then characterized at different frequencies to show actuation-recovery cycles under both antagonistic and nonantagonistic (unforced recovery) actuation scenarios (Fig. 4D).
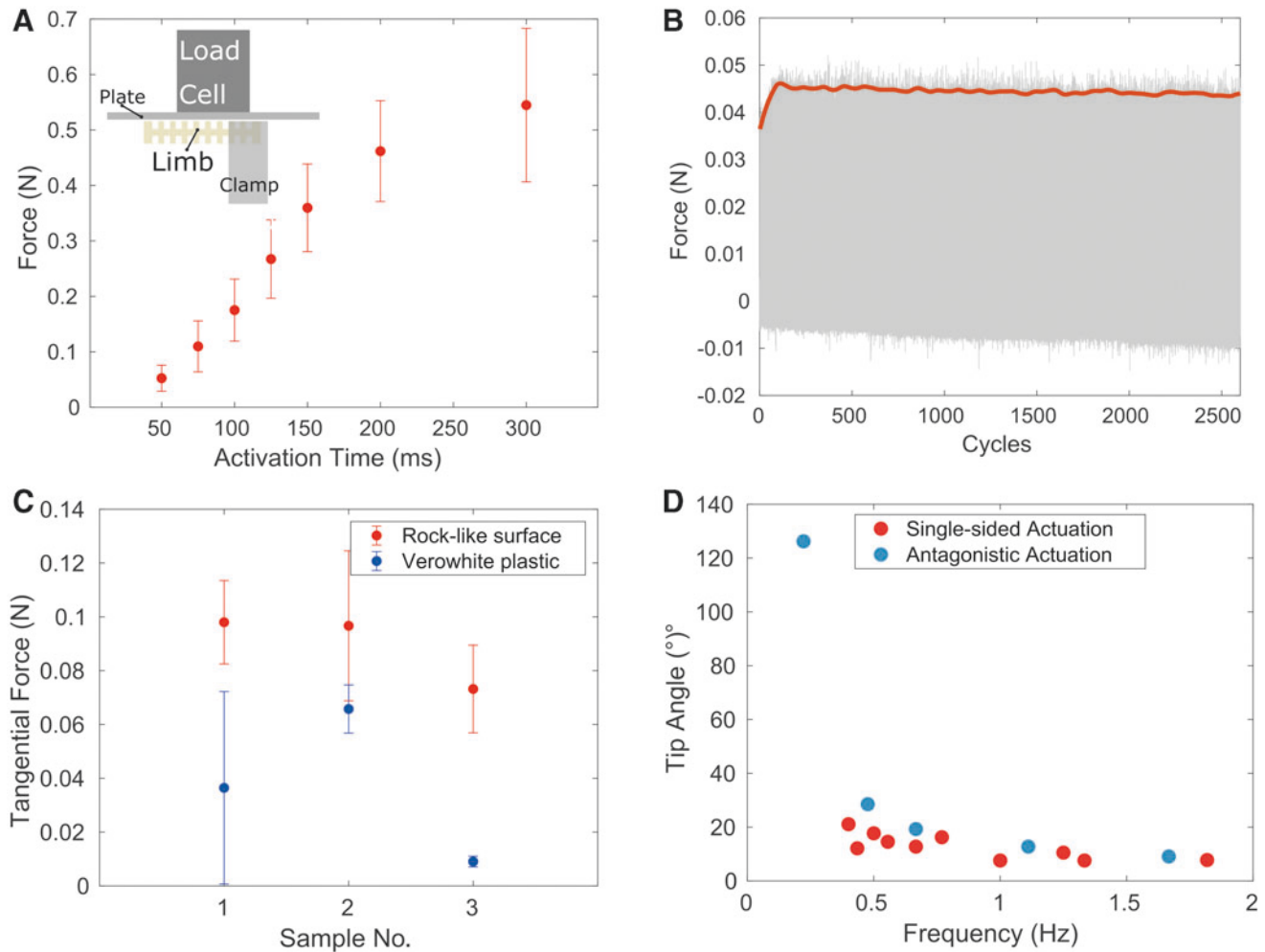
FIG. 4. Characterization. **(A)** Blocking force test results for 11 samples with schematic of test *inset. Error bars* represent standard deviations **(B)** Long-term blocking force test results with a single sample activated for ∼2500 cycles. The *red line* represents a moving average. **(C)** Friction force tests showing the tangential force from single actuators performing the robot gait for a rough and smooth surface. **(D)** Frequency versus angular displacement experiments. Antagonistic actuation refers to trials in which opposing pairs of SMA coils are actuated, whereas single-sided actuation refers to trials in which the opposing pair of coils is not actuated, meaning that all recovery is exclusively due to the passive elasticity of the printed material.

Robot function

The robot's core functionality is to reach a desired location within an underwater environment. The feedback used to accomplish this task is produced by an overhead camera. Using the gait from the previous section as a motion primitive, the robot functions as follows. First, a goal position is chosen by the operator on a remote computer by clicking on the screen. The limb that is most directly pointing toward the goal is then selected as the leading limb and the gait cycle is executed. After this gait cycle, the camera is again used to determine the leading limb. This process repeats until the robot has reached the goal (within an arbitrary threshold). Figure 5 shows a demonstration of this functionality and the corresponding video is shown in Supplementary Movie S1. The robot moves with an average velocity of 0.7204 cm/s, or 0.06 BL/s. This speed is in line with speeds of brittle stars observed in Astley.[31]

After validating the performance of a robot in the laboratory, we built a new one and brought it to a local lake to demonstrate that it can perform in unstructured terrain outside of the laboratory. We note that the color of the fielded robot (shown in Fig. 6) is red. This is a cosmetic change to increase visibility that is induced by adding dye to the 3D printable resin. It has no effect on material properties. The robot was placed in the lake and remotely instructed to perform its previously specified gait in the open loop (see Fig. 6A for setup). The robot moved itself over the flora-covered bottom of the lake, leveraging its flexibility and untethered architecture to avoid being tangled or destroyed in the presence of unmodeled interactions (Fig. 6B). It was closely approached by some local wildlife as well, including the fish shown in Figure 6B and several frogs. For a video of the robot operating in the field, see Supplementary Movie S2.

Discussion and Conclusions

In this study, we used a recently developed 3D printable elastomer to produce an untethered robot that can autonomously navigate to a user-specified location. In Figure 2, we
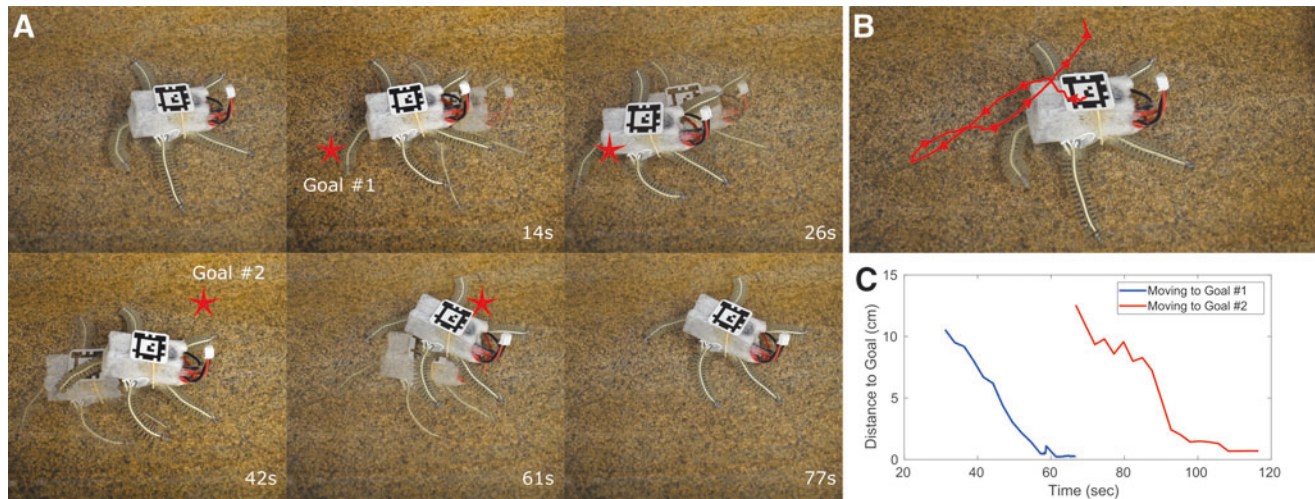
FIG. 5. Robot-controlled demonstration. **(A)** Images of the robot navigating between desired goals, which are simply positions in 2D space commanded by the teleoperator. In *top 3 panels*, the robot moves to the position represented by the *red star* marked Goal #1. After reaching Goal #1, the robot waits for new instructions. The user inputs a new goal position, Goal #2, and the robot navigates to this goal in the *bottom panels*. **(B)** Path followed by the robot. **(C)** Distance to the goal position plotted for the depicted trial. 2D, two-dimensional.

show a visualization of how this study is contextualized and built upon previous work within the field. The combination of highly flexible elastomeric material, untethered design, and high-level feedback-driven motion planning represents a step forward toward 3D printing fully autonomous bioinspired soft robots capable of operation in the real world.

We chose SMA as the actuator because it is relatively compact, has high work density,[32] and is easily integrated

FIG. 6. Operation in a natural aquatic environment. **(A)** Field test setup. **(B)** Robot as it moves along the bed of the lake.

into a fast-moving untethered robot.[33] However, SMA has several limitations that diminish its effectiveness as an actuator for this application, especially low power efficiency and high shape change variability due to environmental conditions, loading, and manufacturing variance.[34] Although we tried to reduce or eliminate these limitations, some are unavoidable. For example, it is likely that small differences in the amount of preload on the actuator during assembly can account for a significant portion of the high variance in force output and angular displacement that we observed across samples, as shown in Figure 4.

This limitation could be mitigated by incorporating on-board sensing to measure states that are relevant to locomotion, such as the curvature of the limbs or the contact forces with the ground.[35] Incorporating such sensors would enable the robot to operate with far more autonomy and would allow controllers to compensate for differences in performance of the actuator. Another possible improvement is to incorporate thermoelectric materials for more precise control of heating and cooling. This could leverage some of the soft thermoelectric material architectures recently introduced by Zadan et al.[36,37]

Even with such drawbacks, our robot was able to function in the field in an aquatic environment. It is also notable that the robot was approached by multiple animals during our experiments, including a frog that used the robot as a hiding spot and a fish that approached within a few centimeters. It has previously been noted that soft robots may be valuable as ecological survey tools because of their relatively limited impact on the environment.[38–40] Our robot seemed to not disturb the wildlife at all, possibly because of its low operating sound and smooth stable motion that avoided the creation of turbulence or turbidity.

Further systematic study is necessary to determine what sort of soft and rigid robots can closely interact with aquatic wildlife, but our result suggests that such a robot may be useful for underwater surveys, particularly in benthic regions with lots of fragile wildlife. Owing to
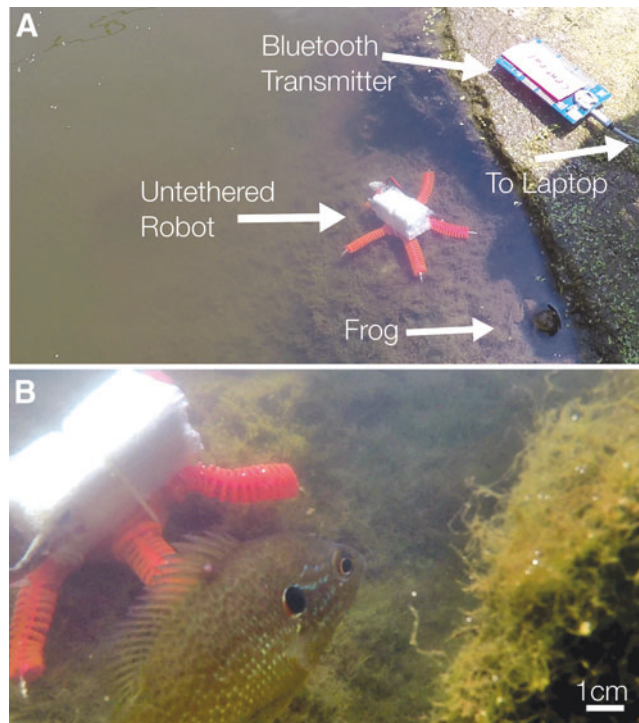
limited access to the lake with available filming equipment, the robot's operation was limited to where we could readily film with a GoPro. Future field tests can use remotely operated tracking and filming technology to explore more remote areas of the lake.

One obvious criticism of the tests is that they are performed in relatively shallow water. During this study, we did not have access to substantially deeper water or a pressurized test setup to test, for example, deep ocean conditions. However, we can see from the existing literature that soft robots perform well at substantial depths.[41] The decrease in performance or outright failure of our robot as we increase depth of operation come from two main factors. First, as characterized in Supplementary Figure S4E, as the temperature drops, the amount of activation time and, therefore, current necessary to achieve substantial actuation rises linearly.

This is easily remedied by using a design that isolates the SMA from the water. Second, as the pressure increases the electronics may fail. When exactly this will occur is hard to say without Finite Element Analysis or experiment, but Li *et al.* provide us with estimates.[42] According to their article, the density of electronics and potting in silicone are the critical factors determining whether the electronics will fail. In this study, distances between components of >2.4 mm are recommended. We are close to this threshold. Also, our circuit is potted in silicone for pressure tolerance.

Another area of improvement is the drop in autonomy in the field. This is due to the use of the benchtop camera for feedback of the robot's position and the use of Bluetooth communication to get that information to the robot. Since the Bluetooth signal attenuates in water, it is unreliable in realistic conditions. One approach from the literature is to instead use acoustic transmission, but this is far too large a payload for a robot at our scale and, furthermore, is very power-hungry. There are two possible approaches that come to mind instead. One is to operate in tandem with a traditional submersible vehicle that can drop our robot into the field, monitor its progress from afar, and get in close to communicate when necessary. However, turbidity in the water and occlusions would be issues with this approach. The other option, one that may be more favorable, is to instead add an inertial measurement unit (IMU) to the robot and estimate the robot's state onboard as best as possible, eliminating the necessity of wireless communication for closed-loop navigation.

In closing, we have shown that we can rapidly fabricate and deploy untethered and autonomous soft robots. This is enabled through the use of DLP-based 3D printing to create rubber-like actuators with complex miniaturized features not possible with 2.5D elastomer molding. As in[19] and other soft robot implementations that involve AM, we note that not all elements of the robot were produced with 3D printing. Only the elastomeric limbs and the main body (to carry electronics) are 3D printed with DLP and the SMA coils, circuit board, battery, and microelectronics are all incorporated later in the manufacturing process. As soft actuator and printed electronics and battery technologies continue to advance, along with advances in soft matter computation and power transmission,[43] it could eventually be possible to create untethered mobile soft robots that are composed entirely of 3D printed materials.

Supplementary Material

Supplementary Data
Supplementary Figure S1
Supplementary Figure S2
Supplementary Figure S3
Supplementary Figure S4
Supplementary Figure S5
Supplementary Figure S6
Supplementary Figure S7
Supplementary Figure S8
Supplementary Table S1
Supplementary Movie S1
Supplementary Movie S2

References

1. Rus D, Tolley MT. Design, fabrication and control of soft robots. Nature 2015;521:467–475.
2. Trivedi D, Rahn CD, Kier WM, *et al.* Soft robotics: biological inspiration, state of the art, and future research. Appl Bionics Biomech 2008;5:99–117.
3. Lipson H. Challenges and opportunities for design, simulation, and fabrication of soft robots. Soft Robot 2014;1: 21–27.
4. Paley DA, Wereley NM. Introduction. In: Paley DA, Wereley NM, eds. Bioinspired Sensing, Actuation, and Control in Underwater Soft Robotic Systems. Cham, Switzerland: Springer International Publishing, 2021, pp. 1–6.
5. Majidi C. Soft robotics: a perspective—current trends and prospects for the future. Soft Robot 2014;1:5–11.
6. Bell MA, Cattani L, Gorissen B, *et al.* A soft, modular, and bi-stable dome actuator for programmable multi-modal locomotion. In: 2020 IEEE/RSJ International Conference on Intelligent Robots and Systems (IROS), Las Vegas, NV, October 24, 2020–January 24, 2021; IEEE, 2020, pp. 6529–6535.
7. Cho KJ, Koh JS, Kim S, *et al.* Review of manufacturing processes for soft biomimetic robots. Int J Precis Eng Manuf 2009;3:171–181.
8. Schmitt F, Piccin O, Barbé L, *et al.* Soft robots manufacturing: a review. Front Robot AI 2018;5:84.
9. Gul JZ, Sajid M, Rehman MM, *et al.* 3D printing for soft robotics—a review. Sci Technol Adv Mater 2018;19:243–262.
10. Stano G, Percoco G. Additive manufacturing aimed to soft robots fabrication: a review. Extreme Mech Lett 2021;42: 101079.

11. Wallin TJ, Pikul J, Shepherd RF. 3D printing of soft robotic systems. Nat Rev Mater 2018;3:84–100.

12. Hinton TJ, Hudson A, Pusch K, et al. 3D printing PDMS elastomer in a hydrophilic support bath via freeform reversible embedding. ACS Biomater Sci Eng 2016;2:1781–1786.

13. Tumbleston JR, Shirvanyants D, Ermoshkin N, et al. Continuous liquid interface production of 3D objects. Science 2015;347:1349–1352.

14. Zheng X, Lee H, Weisgraber TH, et al. Ultralight, ultrastiff mechanical metamaterials. Science 2014;344:1373–1377.

15. Zheng X, Smith W, Jackson J, et al. Multiscale metallic metamaterials. Nat Mater 2016;15:1100–1106.

16. Patel DK, Sakhaei AH, Layani M, et al. Highly stretchable and UV curable elastomers for digital light processing based 3D printing. Adv Mater 2017;29:1606000.

17. Patterson ZJ, Sabelhaus AP, Chin K, et al. An untethered brittle star-inspired soft robot for closed-loop underwater locomotion. In: 2020 IEEE/RSJ International Conference on Intelligent Robots and Systems (IROS), 2020, pp. 8758–8764.

18. Rich SI, Wood RJ, Majidi C. Untethered soft robotics. Nat Electron 2018;1:102–112.

19. Wehner M, Truby RL, Fitzgerald DJ, et al. An integrated design and fabrication strategy for entirely soft, autonomous robots. Nature 2016;536:451–455.

20. Richter C, Lipson H. Untethered hovering flapping flight of a 3D-printed mechanical insect. Artif Life 2011;17:73–86.

21. Phamduy P, Vazquez MA, Kim C, et al. Design and characterization of a miniature free-swimming robotic fish based on multi-material 3D printing. Int J Intell Robot Appl 2017;1:209–223.

22. Joyee EB, Szmelter A, Eddington D, Pan Y. 3D printed biomimetic soft robot with multimodal locomotion and multifunctionality. Soft Robot 2022;9:1–13.

23. Bartlett NW, Tolley MT, Overvelde JTB, et al. A 3D-printed, functionally graded soft robot powered by combustion. Science 2015;349:161–165.

24. Keneth ES, Kamyshny A, Totaro M, et al. 3D printing materials for soft robotics. Adv Mater 2021;33:2003387.

25. Drotman D, Ishida M, Jadhav S, et al. Application-driven design of soft, 3-D printed, pneumatic actuators with bellows. IEEEASME Trans Mechatron 2019;24:78–87.

26. Umedachi T, Vikas V, Trimmer BA. Softworms: the design and control of non-pneumatic, 3D-printed, deformable robots. Bioinspir Biomim 2016;11:025001.

27. Zatopa A, Walker S, Menguc Y. Fully soft 3D-printed electroactive fluidic valve for soft hydraulic robots. Soft Robot 2018;5:258–271.

28. Walters P, McGoran D. Digital fabrication of ''smart'' structures and mechanisms—Creative applications in art and design. NIP Digit Fabr Conf 2011;2011:185–188.

29. Lutken CF. A Contribution to Knowledge of Serpent Stars. II. Overview of the West Indian Ophiurs [in Danish]. Scientific Announcements From the Danish Society for Natural History Copenhagen 1856;7:1–19.

30. Wang J, Olson E. AprilTag 2: efficient and robust fiducial detection. In: 2016 IEEE/RSJ International Conference on Intelligent Robots and Systems (IROS), 2016, pp. 4193–4198.

31. Astley HC. Getting around when you're round: quantitative analysis of the locomotion of the blunt-spined brittle star, Ophiocoma echinata. J Exp Biol 2012;215:1923–1929.

32. Velez C, Patel DK, Kim S, et al. Hierarchical integration of thin-film NiTi actuators using additive manufacturing for microrobotics. J Microelectromechanical Syst 2020;29:867–873.

33. Huang X, Kumar K, Jawed MK, et al. Highly dynamic shape memory alloy actuator for fast moving soft robots. Adv Mater Technol 2019;4:1800540.

34. Huang X, Ford M, J. Patterson Z, et al. Shape memory materials for electrically-powered soft machines. J Mater Chem B 2020;8:4539–4551.

35. Patterson ZJ, Sabelhaus AP, Majidi C. Robust control of a multi-axis shape memory alloy-driven soft manipulator. IEEE Robot Autom Lett 2022;7:2210–2217.

36. Zadan M, Malakooti MH, Majidi C. Soft and stretchable thermoelectric generators enabled by liquid metal elastomer composites. ACS Appl Mater Interfaces 2020;12:17921–17928.

37. Zadan M, Patel DK, Sabelhaus AP, et al. Liquid crystal elastomer with integrated soft thermoelectrics for shape memory actuation and energy harvesting. Adv Mater 2022;34:2200857.

38. Katzschmann RK, DelPreto J, MacCurdy R, et al. Exploration of underwater life with an acoustically controlled soft robotic fish. Sci Robot 2018;3:aar3449.

39. Galloway KC, Becker KP, Phillips B, et al. Soft robotic grippers for biological sampling on deep reefs. Soft Robot 2016;3:23–33.

40. Sinatra NR, Teeple CB, Vogt DM, et al. Ultragentle manipulation of delicate structures using a soft robotic gripper. Sci Robot 2019;4:eaax5425.

41. Aracri S, Giorgio-Serchi F, Suaria G, et al. Soft robots for ocean exploration and offshore operations: a perspective. Soft Robot 2021;8:625–639.

42. Li G, Chen X, Zhou F, et al. Self-powered soft robot in the Mariana Trench. Nature 2021;591:66–71.

43. Hubbard JD, Acevedo R, Edwards KM, et al. Fully 3D-printed soft robots with integrated fluidic circuitry. Sci Adv 2021;7:eabe5257.

44. Umedachi T, Trimmer BA. Design of a 3D-printed soft robot with posture and steering control. In: 2014 IEEE International Conference on Robotics and Automation (ICRA), 2014, pp. 2874–2879.

Address correspondence to:
Carmel Majidi
Department of Mechanical Engineering
Carnegie Mellon University
Pittsburgh, PA 15213
USA

E-mail: cmajidi@andrew.cmu.edu